doi:10.1038/nature11229

## Supplementary Methods

**1.** The eddy was selected on the basis of satellite altimetry and surface chlorophyll distributions. Fertilization was carried out by releasing 7 tonnes of commercial ferrous sulphate dissolved in 54 $m^3$ of acidified (HCl) seawater into the ship's propeller wash while spiralling out from a drifting buoy at 0.9 km radial intervals. By day 14 the initial 167 $km^2$ patch had spread and an area of 740 $km^2$ was again fertilized with 7 tonnes of $FeSO_4$, this time along east-west transects 3 km apart moving downstream from north to south in the direction of the patch (Fig. 1 c).

The patch was located with the drifting buoy and by continuous measurements of the photochemical efficiency ($F_v/F_m$) using a Fast Repetition Rate Fluorometer (FastTracka, Chelsea Instruments) since, as in previous experiments, $F_v/F_m$ was significantly higher in iron-fertilized water. Within a week the bloom had accumulated sufficient biomass so that additional tracers (chlorophyll and online $fCO_2$ concentrations) were used to locate the part of the patch least affected by dilution with outside water, i.e. with the highest chlorophyll and, in the last week, the lowest $fCO_2$ concentrations (Fig 1 c-f). All in-stations were placed inside this "hotspot" and care was taken to locate it with small-scale surveys prior to sampling and to keep the ship within it during the stations which generally lasted about 8 hours. Some in-stations and casts, although within the patch but subsequently shown to have missed the hotspot, have been excluded. For logistical reasons, the out-stations were taken in different locations of the eddy core relative to the direction of the moving patch, i.e. "ahead", "behind" or diagonally opposite it.

**2. Eddy circulation and drift of the patch**

Vertical profiles of ocean currents down to roughly 300 m depth were measured with a vessel-mounted acoustic Doppler current profiler (VM-ADCP, 150 kHz, manufactured by RDI). Processing of the VM-ADCP data was done using the CODAS software package (developed by E. Firing and colleagues, SOEST, Hawaii). The velocity components in geographical coordinates were determined by taking into account the attitude of the ADCP transducer head, its tilt, heading, motion and the geographic position recorded by the ship's navigation system. Only velocity measurements taken at stations were used in the further analysis. The stream function was calculated by first optimally interpolating VM-ADCP velocities onto a regular grid, differentiating to obtain the vorticity and then solving the Poisson equation with gradient boundary conditions. The drift of the patch was tracked by a surface spar buoy equipped with 2 GPS receivers and GPS/Radio as well as GPS/ARGOS modules to record and transmit its geographic position. An 8 m long and 1.2 m wide drogue (Pat.-Nr. DE 10149025 C1), placed between 20 and 30 m depth and connected to the surface buoy by a strong but elastic line, forced the buoy to drift with the mixed layer.

**3. $CO_2$ system measurements**

The $CO_2$ fugacity in seawater was measured by means of an infra-red gas analyser (Li-Cor 6262) coupled to an equilibrator[1] that was linked to the on-line shipboard seawater supply. Atmospheric $fCO_2$ was measured using the same infra-red analyser from air drawn from an airline leading from the crow's nest. Temperature in the equilibrator was measured using a platinum RTD digital thermometer. Temperature at the seawater intake at the bow was measured by ship's equipment (Sea Bird SBE-38 temperature sensor) and logged directly from the ship's data system. The system was calibrated before and after water analyses with air standards with nominal mixing ratios of 0, 202, 348 and 434 ppm $CO_2$. Total alkalinity ($A_T$) was measured by using a VINDTA system adopting the classical Gran electro-titration

method[2]. The reproducibility of measurements was usually within 2 μmol $kg^{-1}$. Dissolved inorganic carbon (DIC) was measured by coulometric titration[3] using a SOMMA system with gas loop calibration with a reproducibility of 2 μmol $kg^{-1}$. Both $A_T$ and DIC were calibrated against certified reference materials from Andrew Dickson at Scripps Institution of Oceanography (SIO).

**4. POC, PON, POP and BSi**

Samples for particulate organic carbon and nitrogen (POC and PON) were filtered onto pre-combusted Whatman GF/F filters and processed following recommendations by Lorain et al.[4]. Samples were measured independently on three different analysers: a CN2500 CHN Analyser (Thermo Finnigan MAT) coupled to a Delta+ mass spectrometer (Thermo Finnigan MAT) via Conflo II interface (Thermo Finnigan MAT), a Carlo-Erba NA-1500 Series II elemental analyzer coupled to a Finnegan Delta+ mass spectrometer and a Euro EA Elemental Analyser (for the latter see Hoffmann et al.[5]). Differences due to methods were within the range of measurement variability (below 2%). The particulate organic phosphorus (POP) content was determined colorimetrically using the method from Hansen and Koroleff[6] (measurement variability 4%). Biogenic silica (BSi) was measured colorimetrically following the wet alkaline digestion method according to Müller and Schneider[7] (measurement variability 2%)

**5. Nutrients, DOC, DON and DOP**

Inorganic nutrients (silicate, phosphate, nitrate, nitrite and ammonium) were measured with a Technicon Autoanalyser II system using standard methods. Dissolved organic carbon (DOC) was determined by high temperature combustion using a TOC-VCPH/CPN (Shimadzu) according to Skoog et al.[8]. Dissolved organic nitrogen and phosphorous (DON and DOP) were measured on a Technicon Autoanalyser II after Valderrama[9]. Precision of nutrient measurements based on repeated analyses of reference standards were 0.4 μM for nitrate, 0.02 μM for nitrite, 0.2 μ M for ammonium, 0.1 μ M for silicate, and 0.02 μ M for phosphate. Variability of DOC measurements based on analyses of reference material was 2 μM.

**6. Chlorophyll and primary production**

Chlorophyll concentrations were determined using a Turner Design Model 10-AU digital fluorometer. Calibration of the fluorometer was carried out following the JGOFS protocol procedure[10]. Results of the fluorometer calibration diverged by 5% between beginning and end of the cruise. Chl*a* content was calculated using average parameter values from the two calibrations. Measurement uncertainty was estimated from triplicate water samples taken from depths ranging between 10 and 100 m depth and averaged 5% of measured values. Primary production was determined from incorporation of $^{14}C$ primary production according to the method of Steemann Nielsen[11]. Samples were measured with a Liquid Scintillation Counter (LSC, Model Tri-Carb 2100 TR, Packard).

**7. Pigments**

Pigment analyses were performed by high performance liquid chromatography (HPLC). For the determination of pigments, 3 to 12 l of sea water was filtered onto one or two 25 mm Whatman GF/F filters. Further treatment and pigment measurement are described in Hoffmann et al.[5].

**8. Microscopy**

The composition of the plankton community and its waste products (empty and broken diatom cells and faecal pellets) was assessed by inverted light and epifluorescence

microscopy (Axiovert 135 and Axiovert 200, Zeiss, Oberkochen, Germany) according to the method of Throndsen[12]. The different species and groups were measured and their biovolume calculated from equivalent geometrical shapes[13,14,15,16]. The biovolume was converted to cellular carbon content through recommended carbon conversion equations[15,17,18]. Discrete values were converted to water column stocks by trapezoidal integration for a 100 m mixed layer.

## 9. Thorium ($^{234}$Th) and POC/$^{234Th}$ ratios

Seawater was sampled for total $^{234}$Th using Niskin bottles at usually 14 depths between surface and 800-1000 m. Samples were processed following the double-spike and small-volume method of Pike et al.[19] and beta-counted on board and then after six months — for background determination — using low level beta counters (Risø, Denmark). Spikes ($^{229}$Th and $^{230}$Th) were analyzed by ICP-MS and Th yield calculated (89% on average). Samples were calibrated against water samples collected at 2000-3000 m water depth where $^{234}$Th and $^{238}$U are assumed to be in equilibrium. $^{238}$U activity was calculated from salinity[20]. The final relative uncertainty on total decay-corrected $^{234}$Th activity was 3%, as given by deep water sample replicates.

Particles were sampled for POC analysis using both plankton net (55 µm mesh size) and Niskin bottles. Net samples and Niskin samples were filtered on polycarbonate filter (pore size: 1 µm; diameter: 142 mm) for particulate $^{234}$Th and on pre-combusted GFF filter for POC analyses. Particulate $^{234}$Th was processed following Rutgers van der Loeff and Moore[21], POC as described above (Supplementary Methods section 4).

## 10. Carbon and nutrient export estimates

*Export estimated from elemental budgets.*

Terms and processes included in budget estimates are illustrated in Fig. SM.1

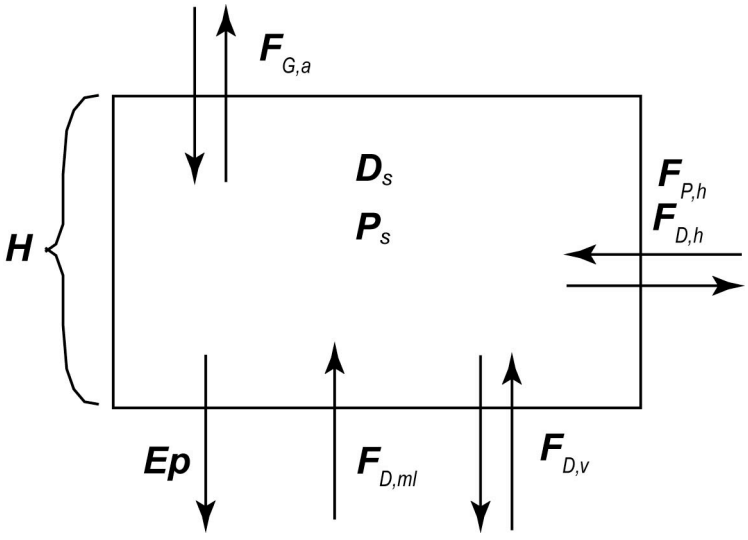


**Figure SM.1.** Surface layer box with biogeochemical processes used in elemental budget estimates. ($H$) Surface layer thickness. ($D_s$, $P_s$) 0 to 100 m depth averaged dissolved and particulate matter concentration, respectively. ($F_{G,a}$) transfer due to air-sea gas exchange. ($F_{D,ml}$) dissolved element entrainment due to wind-induced deepening of the actively mixing layer. ($F_{D,v}$) input of dissolved elements due to diapycnal mixing. ($F_{D,h}$) exchange of dissolved elements due to horizontal mixing (dilution effect). ($F_{P,h}$) exchange of particulate elements due to horizontal mixing (dilution effect). ($Ep$) Vertical flux of particulate matter out of the surface layer.

Mass balance for the surface layer in the hotspot per unit area (1 $m^2$) can be described as

$$H.\,\Delta D_s + H\,.\,\Delta P_s \;=\; F_{G,a} + F_{D,ml} + F_{D,v} \;+ F_{D,h} + F_{P,h} - Ep \qquad 9.1$$

with $H$ = 100 m depth, the surface box thickness, $\Delta D_s$ the change in average surface box dissolved element concentrations and $\Delta P_s$ the change in average surface box particulate element concentrations in the hot-spot, ($F_{G,a}$) the transfer due to air-sea gas exchange (only considered for carbon budgets), $F_{D,ml}$ the dissolved element entrainment due to wind-induced deepening of the actively mixing layer, $F_{D,v}$ the exchange of dissolved elements due to diapycnal mixing, $F_{D,h}$ and $F_{P,h}$ the exchange of dissolved and particulate elements, respectively, due to horizontal mixing (dilution effect) and $Ep$ the vertical export fluxes of particulate matter below the surface layer.
$Ep$ can, therefore, be estimated as:

$$Ep \;=\; F_{G,a} + F_{D,ml} + F_{D,v} \;+ F_{D,h} + F_{P,h} - H.\,\Delta D_s - H\,.\,\Delta P_s \qquad 9.2$$

In this formulation, export of particulate elements due to diapycnal mixing and deepening of the mixing layer are implicitly included in the term $Ep$, which represents total particulate export fluxes below 100 m depth.

Export fluxes $Ep_{(0\text{-}24)}$ below 100 m depth in the hot-spot for the first 24 days of the experiment (between day 0 and day 24 after fertilization, Supplementary Table 2) and for the whole experiment duration $Ep_{(0\text{-}36)}$ (between day 0 and day 36 after fertilization, main text Table 1) were estimated using equation 9.2. The export fluxes due to fertilization $Ep_{ex}$ (main text Table 1) were estimated as the difference between export fluxes for the whole duration of the experiment $Ep_{(0\text{-}36)}$ minus background fluxes estimated by extrapolating export fluxes for the first 24 days to 36 days:

$$Ep_{ex} = Ep_{(0\text{-}36)} - (36/24)\,.\,Ep_{(0\text{-}24)} \qquad 9.3$$

$\Delta D_s$ was calculated as the difference between final (day 24) and initial (day 0) integrated (between 0 and 100 m depth) depth-averaged dissolved elemental concentrations estimated from the linear regression models presented in Fig. 3a-f (main text). The same approach was used for $\Delta D_s$ estimates between day 0 and day 36 except for ammonium and phosphate. In these two cases, values obtained through the linear regression models for day 0 were subtracted from end-values (day 36) calculated from actual measurements. The same approach was used to estimate $\Delta P_s$ between days 0 and 24 (linear regression models presented in Fig. 3g-j). Differences in concentration of particulate elements between day 0 and 36 were estimated by subtracting initial values obtained through the linear regression models for day 0 from final integrated depth-averaged concentrations calculated from actual measurements on day 36.

Carbon budget included input due to $CO_2$ air-sea gas exchange ($F_{G,a}$). Surface fluxes of $CO_2$ were computed from surface concentrations of DIC, alkalinity, atmospheric $fCO_2$ and routine wind speed measurements on board of RV *Polarstern* extrapolated to 10 m as described in Cisewski et al.[22] and following the gas exchange parameterization of Wanninkhof[23] with equilibrium constants of Mehrbach[24] as refitted by Dickson and Millero[25]. We also estimated

air-sea gas exchange using the parameterisation of Nightingale et al.[26] which results in 25% lower $CO_2$ input. The effect on total DIC uptake is 4 % lower.

In cases when the wind-induced actively mixing layer[22] reached below 100 m, input of dissolved elements in the upper 100 m of the water column ($F_{D,ml} = \sum_i F_{D,ml,i}$) were included in elemental budget calculations. $F_{D,ml,i}$ the input of nutrient for each deep mixing (> 100 m depth) event $i$ occurring during the period considered for the budget calculations. $F_{D,ml,i}$ were estimated as $F_{D,ml,i} = I_{0\text{-}Zm,i} \cdot (100/Z_{m,i}) - I_{0\text{-}100,i}$ with $Z_{m,i}$ the depth of the actively mixing layer during mixing event $i$, $I_{0\text{-}Zm,i}$ and $I_{0\text{-}100,i}$ the dissolved element inventories in the layers 0 to $Z_{m,i}$ and 0 to 100 m depth, respectively, prior to each mixing event $i$.

Dissolved element input due to vertical diffusive flux ($F_{D,v}$) was estimated by temporally integrating diffusive fluxes ($K_z \cdot [D_Z\text{-}D_{100}] / [Z\text{-}100]$) with $D_{100}$ and $D_Z$ the dissolved element concentrations measured at 100 m ($D_{100}$) and at Z = 120 m to Z = 140 m depth ($D_Z$) depending on sampling resolution in deeper layers. The vertical diffusivity coefficient used $K_z = 3.3\text{x}10^{-4} \pm 0.8\text{x}10^{-4}$ m$^2$ s$^{-2}$ was determined by Hibbert et al.[27] for the EIFEX eddy.

Horizontal exchange of dissolved ($F_{D,h}$) and particulate ($F_{P,h}$) elements for the surface layer (0-100 m depth) of the hot-spot (dilution effect) was estimated using the fractional change ($f_{t,i}$) in concentration in the hot-spot (Fig. SM.2). $f_{t,i}$ was estimated from the temporal evolution in tracer concentration in the hot-spot assuming an initial tracer concentration in the patch of 1 and an out-patch initial tracer concentration of 0 and using a 2D diffusion model with horizontal diffusivity of 56 m$^2$ s$^{-1}$. The later value was determined using an optimised circulation model for the EIFEX eddy that closely follow patch dilution rate estimates based on consecutive spatial surveys of the patch (Supplementary Information SI.3). A Lagrangian analysis of the eddy core dynamics (Supplementary Information SI. 4) indicates that this approach is appropriate to describe dilution in the patch.

Horizontal exchange of dissolved and particulate matter for the hot-spot were estimated as $F_{D,h} = H \cdot \sum_i f_{t,i} \cdot (D_{out,i}\text{-}D_{in,i})$ and $F_{P,h} = H \cdot \sum_i f_{t,i} \cdot (P_{out,i} - P_{in,i})$ with, $f_{t,i} = f_i \cdot \Delta t_i$, the dimensionless fractional changes in tracer concentration for discrete time intervals $\Delta t_i$ (where $\sum_i \Delta t_i = 24$ or 36, depending on time period considered in the budget), $D_{out,i}$ and $D_{in,i}$ the integrated (0-100 m) depth averaged hot-spot and out-patch dissolved element concentrations, respectively, and $P_{out,i}$ and $P_{in,i}$ the integrated (0-100 m) depth averaged hot-spot and out-patch particulate element concentrations, respectively.

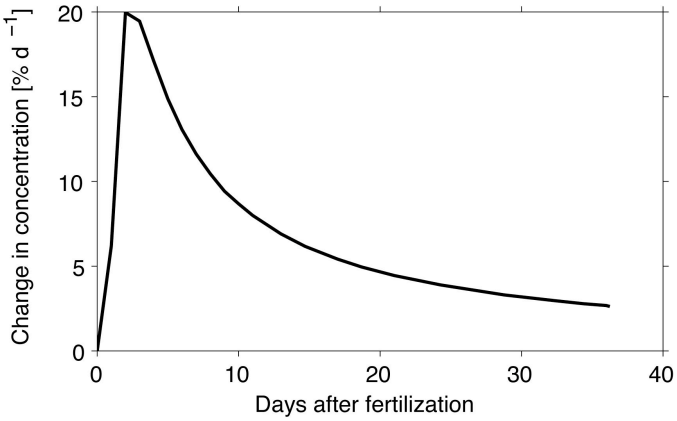


**Figure SM.2.** Temporal evolution of the fractional change in tracer concentration in the hot-spot (here given in % of hot-spot tracer concentration d$^{-1}$) calculated assuming a circular patch with initial area of 167 km$^2$ and a horizontal diffusivity coefficient of 56 m$^2$ s$^{-1}$.

A "conservative" estimate of vertical export fluxes at 100 m depth $Ep_{(0\text{-}36)}$ and $Ep_{ex}$ for the hot-spot (Supplementary Table 1) was estimated using a modified version of equation 9.2 (equation 9.4 below) that does not include horizontal and vertical mixing effects on the budgets.

$$Ep = F_{G,a} - H.\Delta D_s - H.\Delta P_s \qquad 9.4$$

Vertical export fluxes at 100 m depth outside the fertilised patch (Supplementary Table 3) were estimated between days 0 and day 34, when the last out station took place, using the same approach (equation 9.2) but without including horizontal exchange terms ($F_{h,D}$ and $F_{h,P}$) as mixing between eddy and surrounding waters remained low throughout the experiment (see Supplementary Information SI.2 for details on eddy dynamics).

*POC export from light attenuation*

Light attenuation was determined from measurements made with a Wet Labs C-Star transmissometer (660 nm wavelength), which was deployed at hydrographic stations together with the CTD type Sea-Bird Electronics SBE 911plus and a Sea-Bird SBE 32 Carousel multi-bottle water sampler. Prior to calculating light attenuation, the transmissometer readings were corrected for the instrumental drift determined by monitoring the in-air response during the course of the cruise. The attenuation data served two purposes; first, to yield vertical profiles of particulate organic carbon (POC) concentrations derived from the highly significant correlation between attenuation data recorded at the time of closing bottles for the collection of samples and POC concentration in those samples (Supplementary Figure 5). This relationship is valid for the whole water column except for the near-bottom nepheloid layer. Second, to assess the abundance of large particles indicated by the spikes[28] (Supplementary Figure 6) in the high-resolution (24 cycles $m^{-1}$) attenuation profiles.

*POC export fluxes by the $^{234}$Th-deficit approach*

POC export flux was calculated by multiplying the $^{234}$Th flux by the POC:$^{234}$Th (C:Th) ratio of particles of the same depth horizon[29]. Because there was no significant difference between in and out station and between net and Niskin C:Th ratios at 100 m, POC flux at that depth horizon was calculated using a single C:Th ratio of 17.1±3.3 µmol $dpm^{-1}$.

$^{234}$Th fluxes of in-patch stations were calculated using a steady state model during the steady state period (from day 0 to day 20), then using a non-steady state model[30]. Out-patch stations were not sampled in a single body of water, precluding the use of the non-steady state model. Thus, the steady state model was used there. Vertical diffusion and patch horizontal dilution were taken into account for $^{234}$Th flux calculations.

## References

1. Pierrot, D., Neill, C., Sullivan, K., Castle, R., Wanninkhof, R., Lüger, H., Johannessen, T., Olsen, A., Feely, R. and Cosca, C., Recommendations for autonomous underway $pCO_2$ measuring systems and data-reduction routines, *Deep-Sea Res. II* **56,** 512-522 (2009).

2. Gran, G. Determination of the equivalence point in potentiometric titrations of seawater with hydrochloric acid. *Oceanol. Acta* **5**, 209-218 (1952).

3. Johnson, K.M., Williams, P.J., Brandstrom, L. & Sieburth, J. McN. Coulometric total carbon analysis for marine studies: automation and calibration. *Mar. Chem.* **21**, 117-133 (1987).

4. Lorrain, A., Savoye, N., Chauvaud, L., Paulet, Y.-M. & Naulet, N. Decarbonation and preservation method for the analysis of organic C and N contents and stable isotope ratios of low-carbonated suspended particulate material. *Anal. Chim. Acta* **491**, 125, doi:10.1016/S0003-2670(03)00815-8 (2003).

5. Hoffmann, L.J., Peeken, I., Lochte, K., Assmy, P. & Veldhuis, M. Different reactions of Southern Ocean phytoplankton size classes to iron fertilization. *Limnol. Oceanogr.* **51**, 1217-1229 (2006).

6. Hansen, H.P. & Koroleff, F. Determination of nutrients. In *Methods of Seawater Analysis* (eds. K. Grasshoff, K. Kremling & Ehrhard, M.) 159-228. (Wiley-VCH, Weinheim, New York, 1999).

7. Mueller, P.J. & Schneider, R. An automated leaching method for the determination of opal in sediments and particulate matter. *Deep-Sea Res. I* **40**, 425-444 (1993).

8. Skoog, A., Thomas, D., Lara, R. & Richter, K.-U. Methodological investigations on DOC determinations by the HTCO method. *Mar. Chem.* **56**, 39-44 (1997).

9. Valderrama, J. The simultaneous analysis of total nitrogen and total phosphorus in natural waters. *Mar. Chem.* **10**, 109-122 (1981).

10. Knap, A., Michaels, A., Close, A., Ducklow, H. & Dickson A. Measurement of Chlorophyll *a* and Phaeopigments by fluorometric analysis. *JGOFS report* **19**, 118- 122 (1996).

11. Steemann Nielsen, E. The use of radioactive carbon ($C^{14}$) for measuring organic production in the sea. *ICES J. Mar. Sci.* **18**, 117-140 (1952).

12. Throndsen, J. Estimating cell numbers. In *Manual on Harmful Marine Microalgae.* (eds. Hallegraeff, G. M., Anderson, D. M. & Cembella, A. D.) 63-80 (UNESCO, Paris, 1995)..

13. Bé, A. W. H., Hemleben, C., Anderson, O. R., Spindler, M., Hacunda, J. & Tuntivate-Choy, S. Laboratory and field observations of living planktonic foraminifera. *Micropaleontology* **23**, 155-179 (1977).

14. Edler, L. Recommendations for marine biological studies in the Baltic Sea: Phytoplankton and chlorophyll. *The Baltic Marine Biologists publication* **5**, 1-38 (1979).

15. Michaels, A. F., Caron, D. A., Swanberg, N. R., Howse, F. A. & Michaels, C.M. Planktonic sarcodines (Acantharia, Radiolaria, Foraminifera) in surface waters near Bermuda: Abundance, biomass and vertical flux. *J. Plankton Res.* **17**, 131-163 (1995).

16. Hillebrand, H., Duerselen, C. D., Kirschtel, D., Pollingher, U. & Zohary, T. Biovolume calculation for pelagic and benthic microalgae. *J. Phycol.* **35**, 403-424 (1999).

17. Riebesell, U., Reigstad, M., Wassmann, P., Noji, T. & Passow, U. On the trophic fate of Phaeocystis pouchetii (Hariot): 6. significance of Phaeocystis-derived mucus for vertical flux. *Neth. J. Sea Res.* **33**, 193-203 (1995).

18. Menden-Deuer, S. & Lessard, E. J. Carbon to volume relationships for dinoflagellates, diatoms and other protist plankton. *Limnol. Oceanogr.* **45**, 569-579 (2000).

19. Pike, S.M., Buesseler, K. O., Andrews, J. & Savoye, N. Quantification of $^{234}$Th Recovery in Small Volume Sea Water Samples by Inductively Coupled Plasma Mass Spectrometry. *Journal of Radioanalytical and Nuclear Chemistry* **263**, 355-360 (2005).

20. Chen, J. H., Edwards, R. L. & Wasserburg, G. J. $^{238}$U, $^{234}$U and $^{232}$Th in seawater, *Earth Planet. Sci. Lett.* **80**, 241-251 (1986).

21. Rutgers van der Loeff, M. M. & Moore, W.S. Determination of natural radioactive tracers. In *Methods of Seawater Analysis* (eds. K. Grasshoff, M. Ehrhardt & Kremling, K.) 365-397 (Verlag Chemie, Weinheim, 1999).

22. Cisewski, B., Strass, V. H., Losch, M. & Prandke, H. Mixed layer analysis of a mesoscale eddy in the Antarctic Polar Front Zone. *J Geophys. Res.* **113**, doi:10.1029/2007JC004372 (2008).

23. Wanninkhof, R. Relationship between wind speed and gas exchange over the ocean, *J. Geophys. Res.* **97**, 7373-7382 (1992).

24. Mehrbach, C., Culberson, C. H., Hawley, J. E. & Pytkowicz, R. M. Measurement of the apparent dissociation constant of carbonic acid in seawater at atmospheric pressure. *Limnol. Oceanorg.* **18**, 897-907 (1973).

25. Dickson, A.G. & Millero, F.J. A comparison of the equilibrium constants for the dissociation of carbonic acid in seawater media. *Deep-Sea Res.* **34**, 1733-1743 (1987).

26. Nightingale, P.D., Malin, G., Law, C.S., Watson, A.J., Liss,, P.S., Liddicoate, M.I., Boutin, J. & Upstill-Goddard, R.C. In situ evaluation of air-sea gas exchange parameterizations using novel conservative and volatile tracers. *Glob. Biogeochem. Cycles*, **14**, 373-387 (2000).

27. Hibbert, A., Leach, H., Strass, V., & Cisewski, B. Mixing in cyclonic eddies in the Antarctic Circumpolar Current. *J Mar. Res.* **67**, 1-23 (2009).

28. Briggs, N *et al*. High resolution observations of aggregate flux during a sub-polar North Atlantic spring bloom. *Deep-Sea Res. I.* **58**, 1031-1039, doi:10.1016/j.dsr.2011.07.007 (2011).

29. Buesseler, K. O. *et al.* An assessment of particulate organic carbon to thorium-234 ratios in the ocean and their impact on the application of $^{234}$Th as a POC flux proxy. *Mar. Chem.* **100**, 213– 233 (2006).

30. Savoye, N. *et al*. $^{234}$Th sorption and export models in the water column: A review. *Mar. Chem.* **100**, 234-249 (2006).

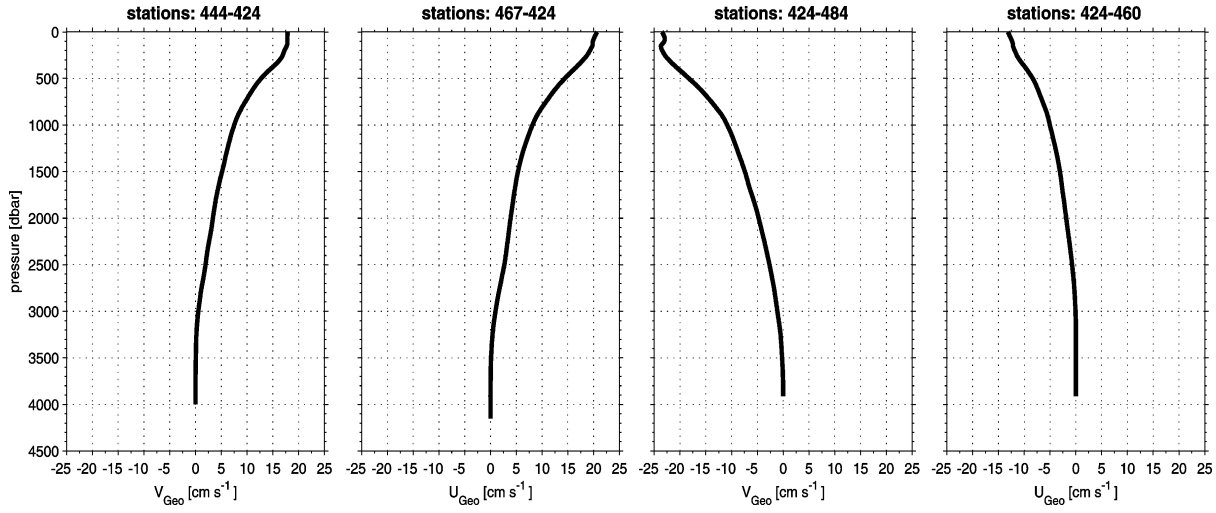


**Supplementary Figure 1. Vertical profiles of geostrophic shear**
U (eastward current) and V (northward current) components of geostrophic shear. Station positions are given in Supplementary Figure 2.

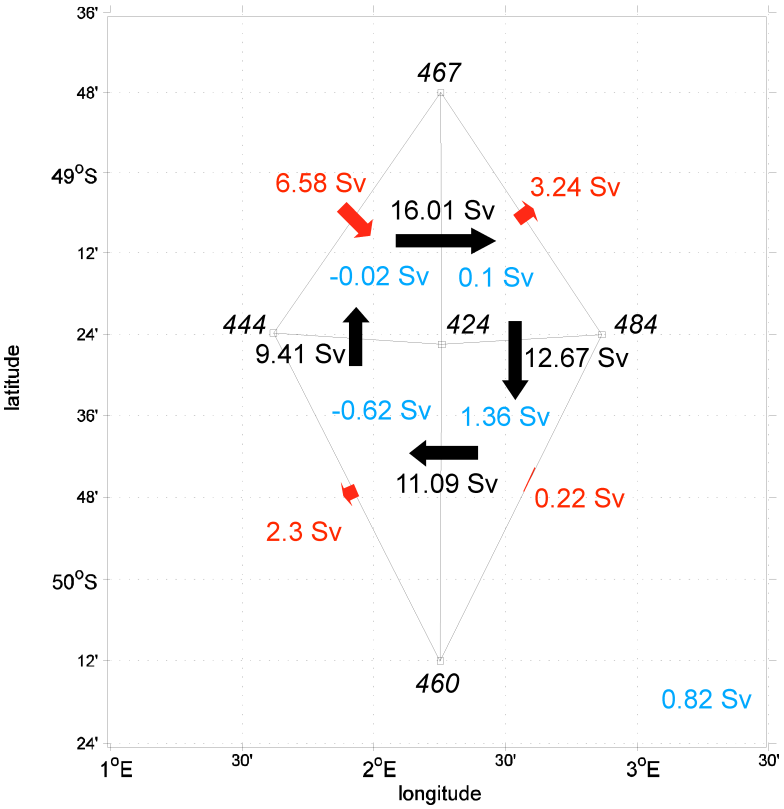


**Supplementary Figure 2. Geostrophic transports.**
Geostrophic transports were calculated relative to the bottom between the deep CTD stations 424, 444, 460, 467 and 484, which were performed between February 11$^{th}$ and 19$^{th}$, 2004. The arrangement of stations, centred around the approximate eddy core (close to station 424), allows for the calculation of the geostrophic flow perpendicular to 8 lines, which each connect one pair of stations. Black arrows and numbers indicate the transports (in units of Sv, 1 Sv = $10^6$ m$^3$ s$^{-1}$) associated with the eddy, red arrows and numbers indicate transports into and out of the array. The largest transports in and out occur in the northern half of the array, where the eddy abuts the eastward flowing Antarctic Polar Front (APF) jet, hence, the transport between stations 467 and 424 (16.01 Sv) includes 3 – 7 Sv contributed by the APF. The blue numbers denote the transport divergence in the four triangles of lines. Summed up, the net divergence, i.e. the imbalance of all transports, is 0.82 Sv. In comparison, an average of about 12.3 Sv circulated with the eddy.

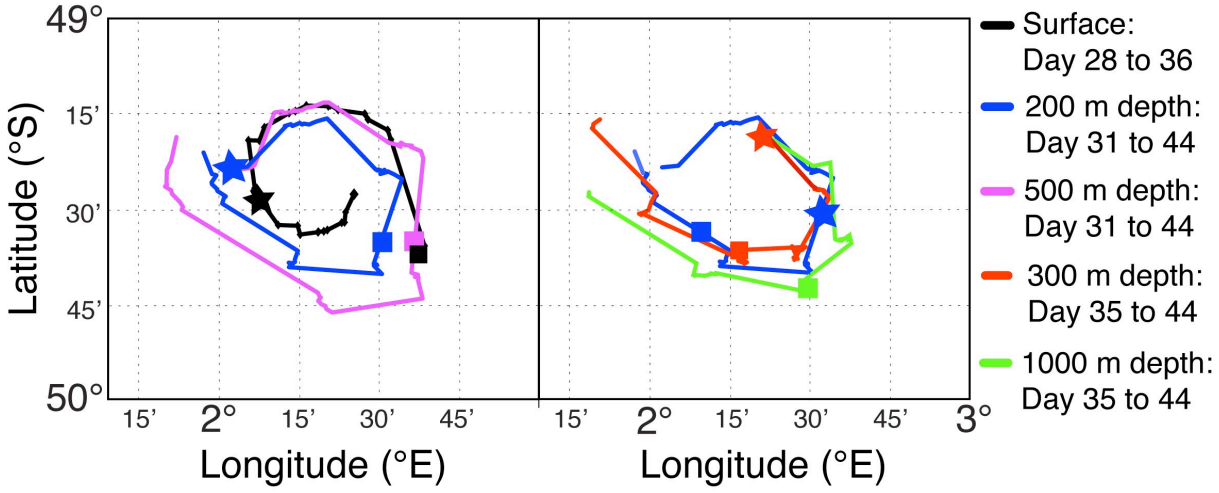


**Supplementary Figure 3. Tracks of surface-tethered buoy and neutrally-buoyant deep floats during the flux event**.
The GPS-equipped buoy (black line) was tethered to a drogue at 30 m depth. It was placed in the hotspot on day 28 but drifted out of it by day 36, although it was still inside the spreading patch. Left panel: Two neutrally buoyant, autonomous floats parked at 200 m (blue line) and 500 m (pink line) were deployed in the hotspot on day 31 (marked with a blue star). The position of the surface buoy at that time is marked with a black star. The position of the buoy and floats on day 36 is marked with the respective coloured squares. Right panel: Two more floats parked at 300 m (red line) and 1,000 m (green line) were deployed in the hotspot on day 35 at the position marked with a red star. The location of the 200 m float at that time is marked with a blue star. The position of the floats on day 41 is marked with the respective coloured squares. The float tracks are reasonably congruent and demonstrate the vertical coherence of the eddy flow field expected from the geostrophic velocities.
The VS-APEX floats (Webb Research Corp.) were programmed for park-and-profile mission. Their respective parking depths at which they rested and drifted with the currents are given above. Once every two days the floats performed a vertical profile by sinking to their common maximum depth of 1500 m. From there the floats ascended to the surface where they stayed for about 10 hours before sinking again to their parking depth.

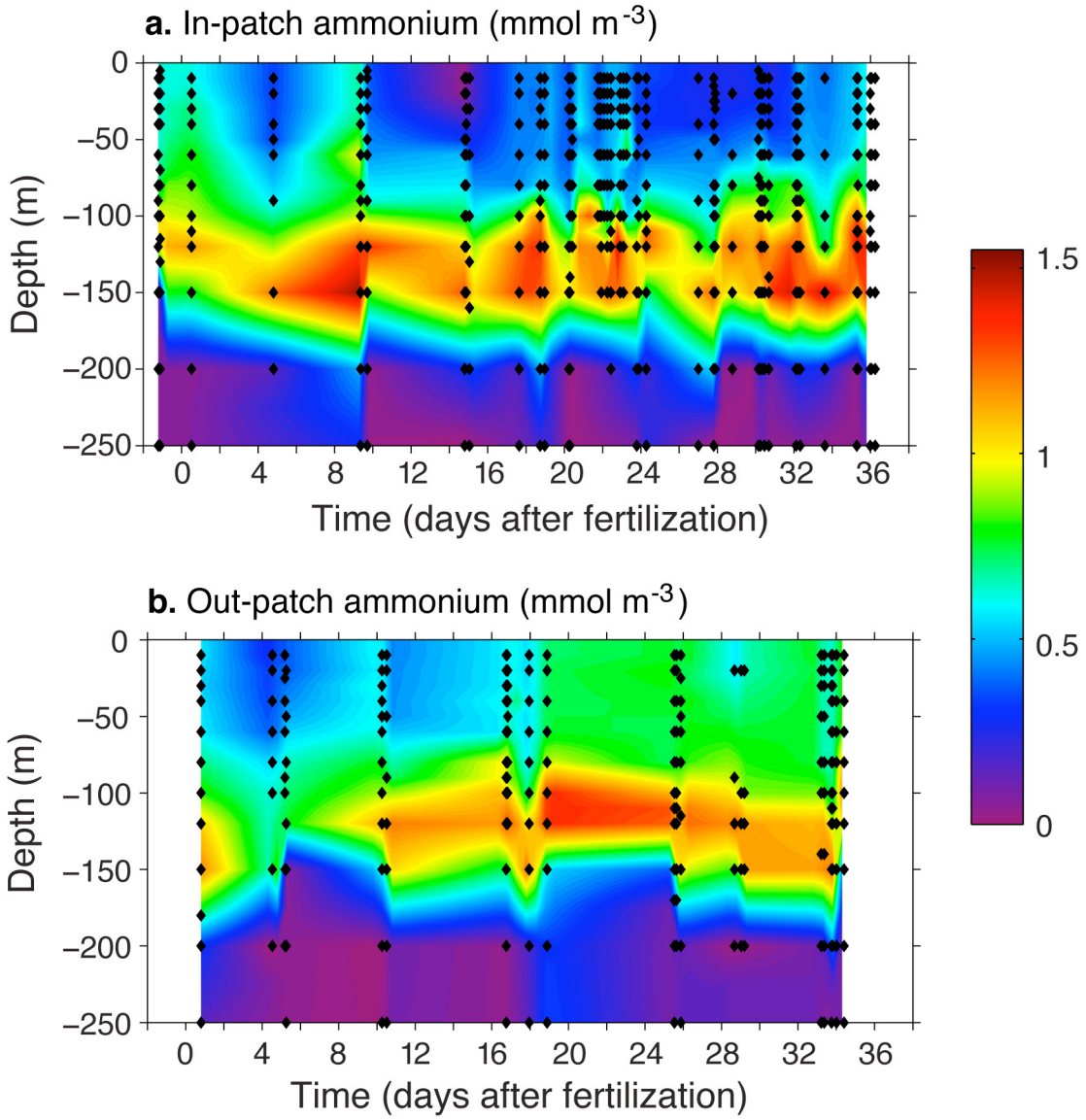


**Supplementary Figure 4. Temporal evolution of ammonium concentrations.**
Note relative lack of change in the subsurface maximum during the demise phase of the bloom and increasing surface layer concentrations outside the patch in the second half of the experiment. Black diamonds in each panel indicate position of discrete samples.

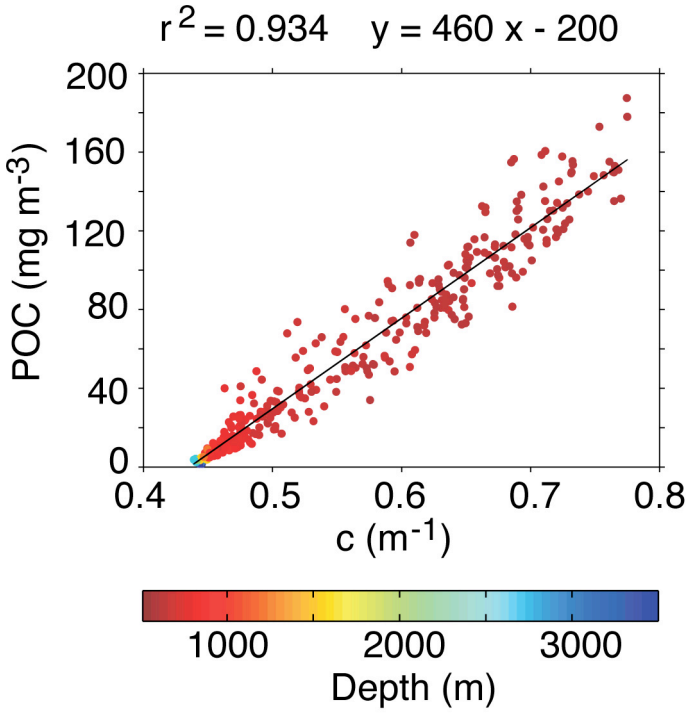


**Supplementary Figure 5. POC versus attenuation.**
Regression analysis of attenuation (c), measured with the transmissometer, versus particulate organic carbon (POC) measured in discrete samples. Correlation coefficient and regression equation are given on top of the panel.

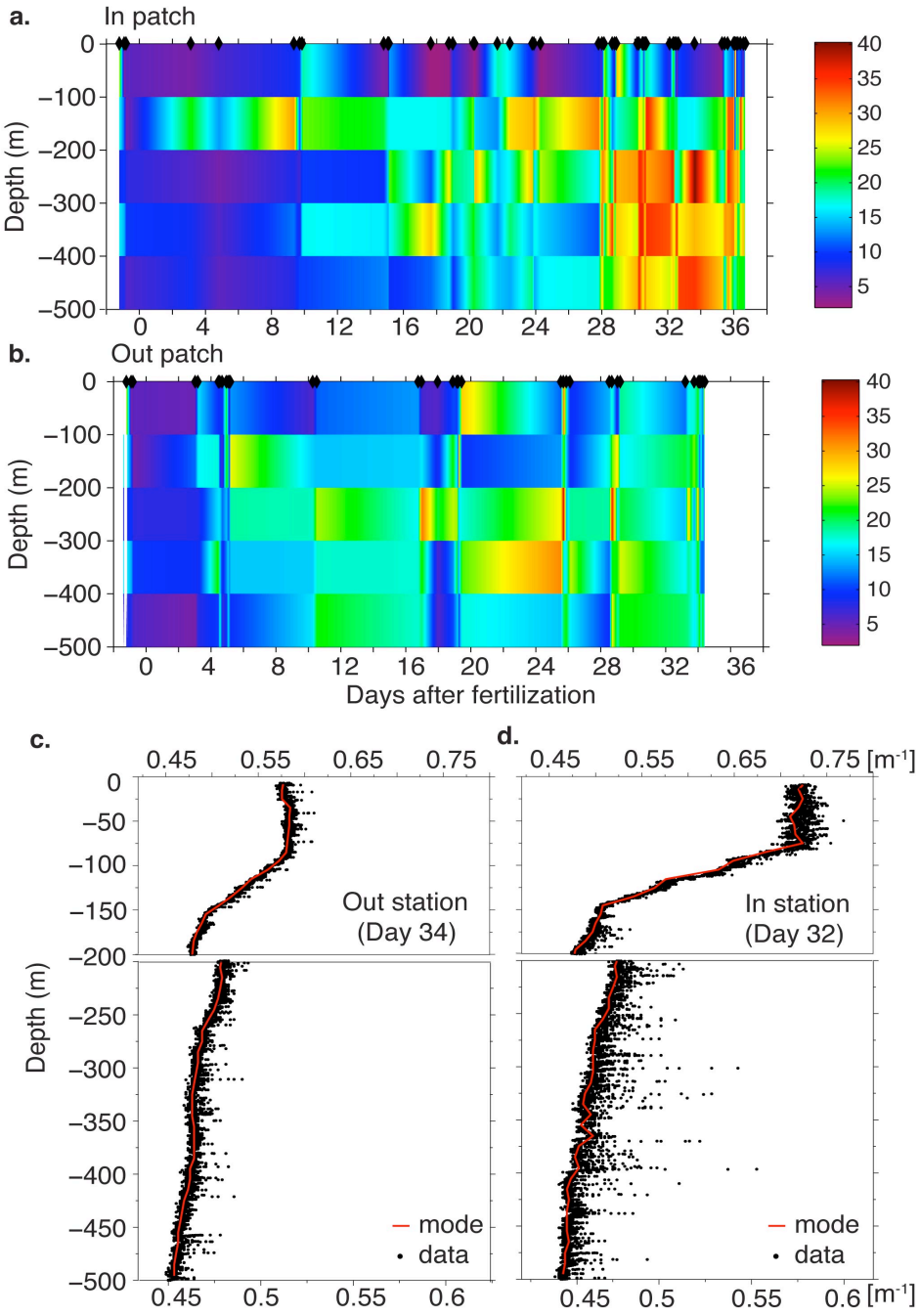


**Supplementary Figure 6. Large aggregates in the upper 500 m during the experiment.** Large aggregates are recorded as the percent contribution of large spikes to light beam attenuation profiles recorded by the transmissometer inside and under the hotspot (a) and outside the patch (b). Large spikes are defined as data points that are larger than the mode + (mode - minimum) attenuation determined in 10 m intervals from the attenuation profile at full resolution of 24 Hz, roughly equivalent to 24 data points per meter.Ten meter intervals contain enough data for a statistical analysis but still result in fine resolution of the vertical structure of the background attenuation (c, d). The percentage of large spikes is subsequently calculated as the proportion of detected spikes to the total amount of data points in 100 m thick layers. The lower panels are transmissometer profiles from 0 – 200 and 200 – 500 m outside the patch taken on day 34 (c), and inside and under the hotspot on day 32 during the flux event (d). Red line indicates the mode. Note the much larger number of spikes under the hotspot. Black diamonds in each panel indicate position of the transmissometer profiles.

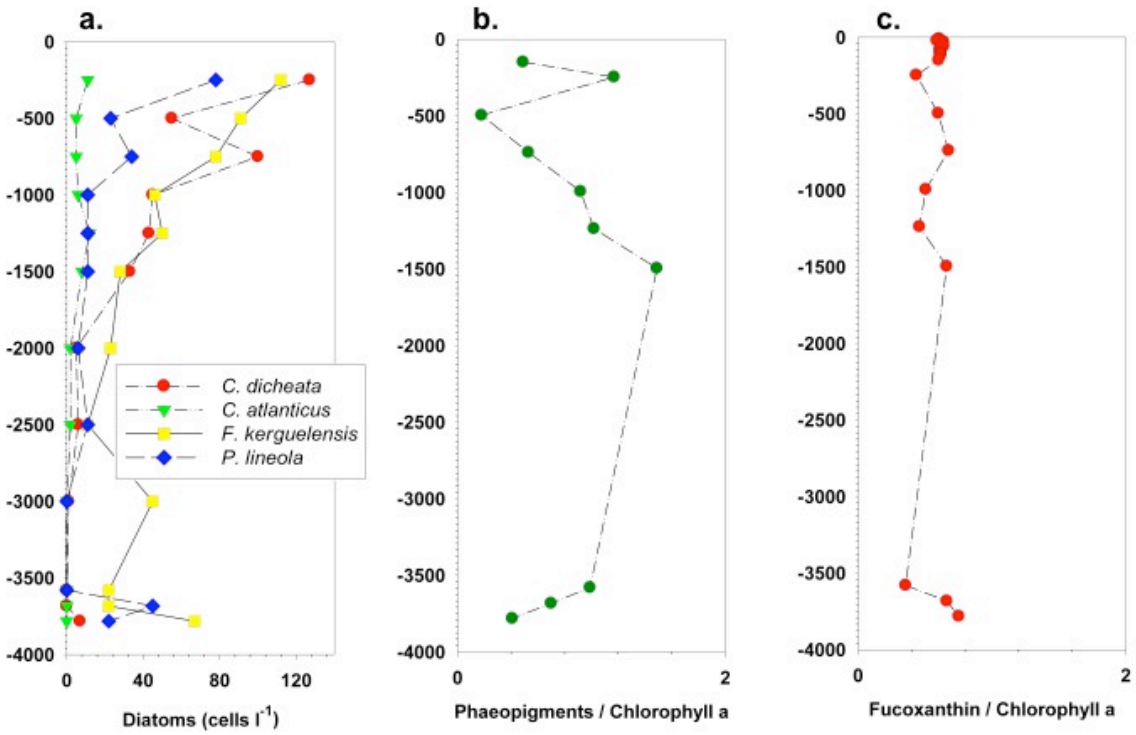


**Supplementary Figure 7. Diatom species and pigment ratios under the patch on Day 36.** a. Vertical distribution of concentrations of frustules of dominant diatom species (*Chaetoceros dichaeta*, *C. atlanticus*, *Fragilariopsis kerguelensis* and *Pseudonitzschia lineola*). The cells were counted in 12 L samples concentrated by passing through a 20 µm mesh sieve. Note higher numbers of *P. lineola* just above the bottom. In contrast to *F. kerguelensis*, this species is not preserved in sediments so their presence close to the bottom indicates freshly settled material. b. Ratios of phaeopigments/chlorophyll *a*, and c. ratios of fucoxanthin/chlorophyll *a* determined from HPLC analyses. The low ratio of phaeopigments/chlorophyll *a* in the near-bottom layer signal the presence of freshly deposited phytoplankton, while the high ratio of fucoxanthin/chlorophyll *a* at depth reflects the dominance of diatoms during the flux event.

**Supplementary Table 1. Hotspot elemental budgets based on measured stocks without correction for diapycnal and horizontal mixing.**

| Days | Si | P | $NO_2$+$NO_3$ | Total N | C |
|---|---|---|---|---|---|
| Decrease in stocks of dissolved elements | | | | | |
| 0-36 | 1.14 ± 0.03 | 0.007 ± 0.003 | 0.160 ± 0.008 | 0.33 ± 0.08 | 1.1 ± 0.2 |
| Input due to air-sea gas exchange | | | | | |
| 0-36 | - | - | - | - | 0.4 |
| Difference between final and initial particulate matter standing stocks | | | | | |
| 0-36 | 0.28 ± 0.02 | 0.0062 ± 0.0005 | 0.081 ± 0.009 | 0.081 ± 0.009 | 0.11 ± 0.07 |
| **Vertical export (difference in stocks of dissolved elements - difference in particulate stocks)** | | | | | |
| 0-36 | 0.86 ± 0.03 | 0.0011 ± 0.003 | 0.08 ± 0.01 | 0.25 ± 0.08 | 1.4 ± 0.2 |
| Background export* | | | | | |
| 0-36 | 0.46 ± 0.06 | 0.014 ± 0.003 | *-0.06 ± 0.02* | 0.15 ± 0.05 | 0.4 ± 0.2 |
| **Vertical export due to fertilization (vertical export - background export)** | | | | | |
| 24-36 | 0.40 ± 0.07 | -0.013 ± 0.004 | nd | 0.1 ± 0.1 | 0.9 ± 0.3 |

Budgets were calculated for the surface layer (0-100 m) from the beginning of the fertilization experiment (day 0) until the last station carried out inside the fertilized patch (day 36) (see Supplementary Methods for details). Total N includes $NO_2$+$NO_3$, DON and ammonium. All values are in mol $m^{-2}$. Uncertainties (s.e.m.) were estimated by propagation of standard errors based on linear uptake models (Fig. 3) and measurement uncertainties.

* Vertical export between days 0 to 24 (0.3 mol C $m^{-2}$) extrapolated to 36 days.

**Supplementary Table 2. Hotspot elemental budgets for Days 0 to Day 24.**

| Days | Si | P | $NO_2$+$NO_3$ | Total N | C |
|---|---|---|---|---|---|
| Decrease in stocks of dissolved elements | | | | | |
| 0-24 | 0.77 ± 0.02 | 0.017 ± 0.002 | 0.107 ± 0.007 | 0.25 ± 0.03 | 0.7 ± 0.1 |
| Input due to air-sea gas exchange | | | | | |
| 0-24 | - | - | - | - | 0.2 |
| Dissolved element input from vertical mixing (diapycnal mixing and deepening of the mixing layer) | | | | | |
| 0-24 | 0.111 ± 0.007 | 0.0069 ± 0.0008 | 0.028 ± 0.007 | 0.04 ± 0.01 | 0.3 ± 0.1 |
| Dissolved element input from horizontal mixing (dilution effect) | | | | | |
| 0-24 | | 0.0057 ± 0.0009 | 0.032 ± 0.005 | 0.039 ± 0.005 | 0.07 ± 0.06 |
| **Total uptake (decrease of dissolved stocks + gas exchange + vertical mixing + horizontal mixing)** | | | | | |
| 0-24 | 0.88 ± 0.03 | 0.030 ± 0.002 | 0.17 ± 0.01 | 0.33 ± 0.03 | 1.4 ± 0.2 |
| Difference between final and initial particulate matter standing stocks | | | | | |
| 0-24 | 0.46 ± 0.03 | 0.0077 ± 0.0008 | 0.15 ± 0.01 | 0.15 ± 0.01 | 0.7 ± 0.1 |
| Particulate matter loss by horizontal mixing (dilution effect) | | | | | |
| 0-24 | 0.09 ± 0.02 | 0.0050 ± 0.0004 | 0.061 ± 0.006 | 0.0605 ± 0.0004 | 0.35 ± 0.03 |
| **Vertical export (Total uptake - difference in particulate stocks - particulate loss by horizontal mixing)** | | | | | |
| 0-24 | 0.33 ± 0.05 | 0.017 ± 0.002 | -0.04 ± 0.02 | 0.12 ± 0.04 | 0.4 ± 0.2 |

Budgets were calculated for the surface layer (0-100 m) from the beginning of the fertilization experiment (day 0) until day 24 (see Supplementary Methods for details). Total N includes $NO_2$+$NO_3$, DON and ammonium. All values are in mol $m^{-2}$. Uncertainties (s.e.m.) were estimated by propagation of standard errors based on linear uptake models (Fig. 3) and measurement uncertainties.

**Supplementary Table 3. Out-patch elemental budgets**

| Days | Si | P | $NO_2$+$NO_3$ | Total N | C |
|---|---|---|---|---|---|
| Decrease in stocks of dissolved elements | | | | | |
| 0-34 | 0.81 ± 0.09 | 0.004 ± 0.002 | 0.04 ± 0.01 | 0.22 ± 0.07 | 0.1 ± 0.1 |
| Input due to air-sea gas exchange | | | | | |
| 0-34 | - | - | - | - | 0.15 |
| Dissolved element input from vertical mixing (diapycnal mixing and deepening of the mixing layer) | | | | | |
| 0-34 | 0.23 ± 0.02 | 0.0057 ± 0.0004 | 0.050 ± 0.004 | 0.05 ± 0.02 | 0.50 ± 0.09 |
| **Total uptake (decrease of dissolved stocks + gas exchange + vertical mixing + horizontal mixing)** | | | | | |
| 0-34 | 1.04 ± 0.09 | 0.010 ± 0.002 | 0.09 ± 0.01 | 0.27 ± 0.07 | 0.8 ± 0.2 |
| Difference between final and initial particulate matter standing stocks | | | | | |
| 0-34 | -0.02 ± 0.06 | -0.007 ± 0.001 | -0.06 ± 0.02 | -0.06 ± 0.02 | -0.42 ± 0.07 |
| **Vertical export excluding inputs due to vertical mixing (decrease in dissolved elements + gas exchange - change in particulate)** | | | | | |
| 0-34 | 0.8 ± 0.1 | 0.011 ± 0.002 | 0.10 ± 0.02 | 0.28 ± 0.07 | 0.7 ± 0.1 |
| **Vertical export including inputs due to vertical mixing (Total uptake - change in particulate)** | | | | | |
| 0-34 | 1.1 ± 0.1 | 0.017 ± 0.002 | 0.15 ± 0.02 | 0.33 ± 0.07 | 1.2 ± 0.2 |

Budgets were calculated for the surface layer (0-100 m) from the beginning of the fertilization experiment (day 0) until the last station carried out outside the fertilized patch (day 34) (see Supplementary Methods for details). Total N includes $NO_2$+$NO_3$, DON and ammonium. All values are in mol $m^{-2}$. Uncertainties (s.e.m.) were estimated by propagation of standard errors based on linear uptake models (Fig. 3) and measurement uncertainties.